INORGANIC CHEMISTRY

FRONTIERS

Accepted Manuscript

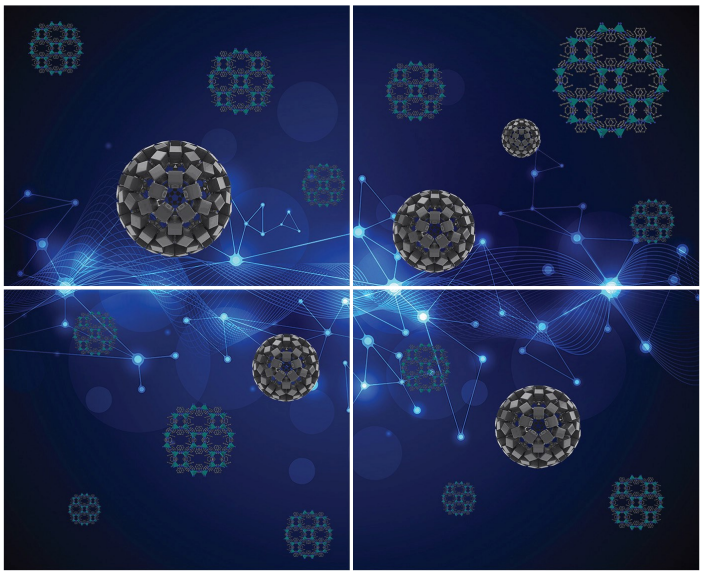

This article can be cited before page numbers have been issued, to do this please use: E. Cariati, D. Malpicci, E. Lucenti, A. Forni, D. Marinotto, A. Previtali, L. CARLUCCI, P. Mercandelli, C. Botta and S. Righetto, *Inorg. Chem. Front.*, 2020, DOI: 10.1039/D0QI01377C.

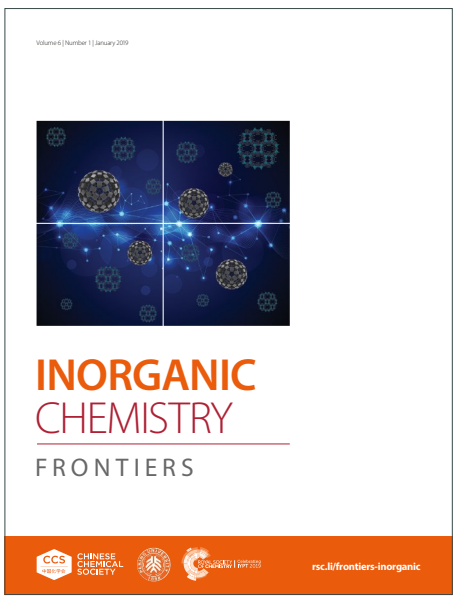

Ag(I) and Cu(I) cyclic-triimidazole coordination polymers: revealing different deactivation channels for multiple room temperature phosphorescences

Received 00th January 20xx,
Accepted 00th January 20xx

DOI: 10.1039/x0xx00000x

Daniele Malpicci,[a] Elena Lucenti,[b] Alessandra Forni,*[b] Daniele Marinotto,[b] Andrea Previtali,[ab] Lucia Carlucci,[a] Pierluigi Mercandelli,[a] Chiara Botta,[c] Stefania Righetto[a] and Elena Cariati*[ab]

The remarkable emissive properties of cyclic triimidazole (**TT**), showing crystallization-induced emissive behavior and, in particular, room temperature phosphorescence (RTP), are here combined with its versatility in assembling coordination compounds. A series of Ag(I) coordination polymers (CPs), comprising a 1D chain ($[Ag(TT)I]_n$, **1-Ag**) and 3D networks ($[Ag(TT)Cl]_n$, **2-Ag**, and $[Ag_3(TT)_4]_n(NO_3)_{3n}\cdot 6nH_2O$, **3-Ag**), have been synthesized and their photophysical behavior thoroughly investigated. They show both fluorescence and multiple RTPs, all simultaneously activated but varied in intensity by changing the excitation energy. Based on DFT/TDDFT calculations and analysis of the X-ray crystal structures, the origin of the different phosphorescences has been ascribed to H-aggregation of the ligand (in **1-Ag** and **2-Ag**), intermolecular electronic coupling by extrinsic heavy-atom effect (in **1-Ag**) and Ligand-Centered emissive states (in all three compounds). Comparison with isostructural **1-Cu** and **2-Cu** CPs reveals that, differently from the Ag(I) analogues, non-thermally equilibrated XMLCT and Ligand-Centered emissive states are active. The isostructural Ag(I) and Cu(I) compounds show comparable emission efficiency, while phosphorescence lifetimes are longer for the former (ms regime) than the latter (μs regime). A Quantum Theory of Atoms in Molecules (QTAIM) topological analysis of electron density allows to interpretate the different nature of the emissive states of Ag(I) and Cu(I) compounds on the basis of larger shell-shared character of the Cu–N bond with respect to the Ag–N one.

Introduction

The fundamental properties of emissive coordination compounds of monovalent coinage d^{10} metals Cu(I), Ag(I) and Au(I), have been the subject of extensive investigation in view of their applications in diverse areas spanning from light-emitting devices to biological sensors.[1-4] In particular, Cu(I) coordination compounds have received remarkable attention due to their usually high quantum efficiency together with practical issues such as the Cu low-cost and natural abundance. Au(I) complexes have been as well largely studied principally owing to the ever-growing interest in gold-catalyzed reactions. Ag(I) compounds, on the other hand, have received less attention mainly owing to their light sensitivity.[5]

The limited number of systematic photophysical studies performed on isostructural Cu(I), Ag(I) and (possibly) Au(I) complexes[5-7] converge on the observation that the heavy-atom effect does not follow the standard trend. Higher ISC rates are in fact frequently observed for complexes of the lighter Cu(I) than for the Ag(I) and Au(I) ones. This result has been explained[7,8] by the observation that the emissive behavior of these complexes is mainly governed by the involvement of the metal d orbitals in the electronic transitions rather than by its atomic number. In fact, the emissive states of Cu(I) complexes have mainly MLCT (metal to ligand charge-transfer) or XMLCT (where X refers to the halogen atom) character, i.e. large metal d contribution. On the contrary, the lower excited states of Ag(I) and Au(I) complexes have mainly ligand-centered (LC) electronic character.

Even fewer studies in this direction have been carried out on d^{10} metal coordination polymers, which are known to display a wide variety of structural formats characterized by strikingly different emissive behavior.[3a,9] Among them, the double-stranded stair-step polymeric structure, $\{MXL\}_n$ (with M = d^{10} metal, X = Cl, Br, I and L = organic ligand), is a quite common motif for Cu(I) compounds and represents a powerful work bench for comparing emissive properties associated with different ligands.[10,11] Though some Ag(I) double-stranded structures have been reported in the past (see [12] and references therein), only a handful of studies, to the best of our knowledge, include the photophysical characterization of the investigated compounds.[13-16] In particular, a deep analysis has been reported on the $[Ag_2(Bmib)I_2]_n$ and $[Ag_2(Bmib)Br_2]_n$ (Bmib standing for 1,4-bis(2-methylimidazol-1-yl)butane) stair polymers,[13] where the ligand was properly chosen to build up Ag(I) coordination network compounds showing excitation wavelength-dependent fluorescence. Such property was ascribed to the flexibility of the long chains of the ligand and the spatial orientation adjustment of the methyl groups at different excitation wavelengths. However, the comparison with isostructural Cu(I) compounds is lacking.

Cyclic triimidazole (**TT**) has revealed[17] to be a useful tecton to prepare coordination compounds thanks to the presence, at the vertexes of a regular triangle, of three nitrogen atoms available for coordination to metal ions. In particular, a thorough

[a] Department of Chemistry, Università degli Studi di Milano and INSTM RU, via Golgi 19, 20133 Milano, Italy.
[b] Institute of Sciences and Chemical Technologies "Giulio Natta" (SCITEC) of CNR, via Golgi 19, 20133 Milano, Italy.
[c] Institute of Sciences and Chemical Technologies "Giulio Natta" (SCITEC) of CNR, via Corti 12, 20133 Milano, Italy.

Electronic Supplementary Information (ESI) available: Experimental and computational details; detailed synthetic procedures and characterization for **1-Ag**, **2-Ag** and **3-Ag**; single-crystal X-ray diffraction data; photophysical data; molecular modeling studies (PDF); X-ray data for 1-Ag (CIF); X-ray data for 2-Ag (CIF); X-ray data for 3-Ag (CIF). See DOI: 10.1039/x0xx00000x

investigation has been reported on the synthesis and structural characterization of an extended series of 1D, 2D and 3D halide coordination networks of Cu(I).[17] Here we extend the versatility of **TT** as monodentate or tridentate ligand to build up, respectively, 1D (**1-Ag**) or 3D (**2** and **3-Ag**) coordination polymers. From a photophysical point of view, **TT** is an interesting dye[18] showing crystallization induced emission behavior, being almost non emissive in solution but highly so as crystalline powders due to concomitant fluorescence and phosphorescence (with lifetimes up to 1 s at room temperature) (overall quantum yield, Φ, equal to 30%). Its ultralong room temperature phosphorescence (RTP) has been explained by the formation of H-aggregates due to strong π-π stacking interactions in the crystal structure. Such aggregation motif has been demonstrated to stabilize the excited triplet state acting as energy trap and then prolonging the deactivation decay rates.[18-20] A systematic photophysical study on **1**-, **2**- and **3-Ag** is here reported and analyzed in comparison with isostructural **1**- and **2-Cu** CPs previously reported[17] and here critically reviewed.

Results and discussion

1D Coordination Polymer $[Ag(TT)I]_n$ (1-Ag)

Crystals of the coordination polymer 1D $[Ag(TT)I]_n$. (**1-Ag**) have been obtained by slow addition of an acetonitrile (CH_3CN) solution of **TT** to a saturated aqueous solution of AgI in KI or to a solution of AgI and KI in *N*,*N*-dimethylformamide (DMF) (see ESI). The compound crystallizes in the monoclinic space group $P2_1/c$. The asymmetric unit contains one silver atom, one **TT** ligand and one iodine atom (Figure 1). Silver atoms are coordinated to three μ_3-I ions and one κ*N*-**TT** ligand in an AgI_3N distorted tetrahedral environment, while the μ_3-I ions adopt a distorted trigonal pyramidal geometry, connecting three different silver atoms. The resulting extended motif is a double-stranded stair chain of $[AgI]_n$ composition which is decorated on both sides by monodentate **TT** ligands [Ag–N 2.319(3) Å]. The chains are built up by Ag_2I_2 parallelograms fused on their two opposite short edges [Ag–I = 2 × 2.8084(5), 2.8682(5), 2.9221(5) Å; I–Ag–I = 109.584(16), 111.927(12), 113.568(12)°] and folded at an angle of 55.24(1)° (dihedral angle between main planes of adjacent Ag_2I_2 units) to give a zig-zag ladder-like arrangement. The short and long diagonals within the Ag_2I_2 parallelograms correspond to Ag···Ag and I···I distances of 3.1591(5) and 4.7499(4) Å], respectively, with the Ag···Ag distance significantly shorter than twice the van der Waals radius of silver (3.44 Å). The **TT** ligands on both sides of the chains are all parallel and superimposed along the crystallographic **b** direction at a distance of 3.1726(19) Å (distance between their mean planes), while the distance between the centroids of their triazine moieties is 4.731(2) Å. The ligands coordinated on the two sides of the same chain are almost orthogonal to each other with an angle between the mean planes of adjacent ligands on opposite sides of 84.22(4)°. All of the chains run along the crystallographic **b** direction. Adjacent chains are held together only by weak C–H···N hydrogen bonds [C5–H4···N5(1 – *x*, 1 – *y*, 1 – *z*) = 3.270(5), C4–H3···N3(1 – *x*, ½ + *y*, 1½ – *z*) = 3.433(5) Å] and by a short contact between the μ_3-iodide and a carbon atom of an imidazole moiety [I1···C2(*x*, ½ – *y*, –½ + *z*) = 3.664(4) Å].

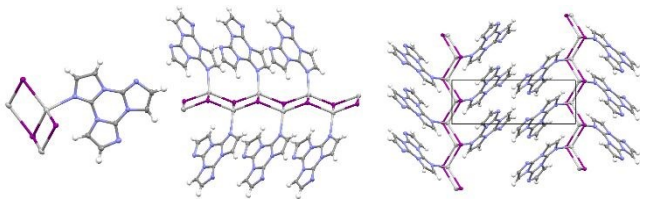

Figure 1. Views of the crystal structure of 1-Ag showing the coordination environment around the silver atoms (left), a single 1D chain (middle), and two chains of opposite chirality viewed along the crystallographic c direction (right). Ellipsoids are drawn at 50% probability.

1-Ag is isostructural and isomorphous to **1-Cu**.[17] The main difference between the two structures is the intra-chain metal-metal distance which is slightly longer than twice the van der Waals radius of the metal for **1-Cu** but quite shorter for **1-Ag**. Comparison of the **TT** arrangement in the two structures shows minor differences and, given the same parallel disposition of **TT** molecules along the **b** axis, similar distances between the heterocyclic ligands can be observed. In particular, the distance between molecular mean planes is 3.1726(19) vs 3.1730(6) Å and the distance between triazine centroids is 4.731(2) vs 4.5090(13) Å for **1-Ag** and **1-Cu**, respectively.

The two structures therefore show the presence of similar H-aggregates and weak C–H···N interactions, while the inter-chain I···C contact previously described is shorter in **1-Ag** than in the copper derivative [3.664(4) vs 3.721 (2) Å]. It is to be noticed that while the $[M_2I_2]_n$ ladder-like motif is very common for Cu(I) derivatives, the same is not true for Ag(I). A search in the CSD database (Ver. 5.41, August 2020) gave only few examples of similar $[Ag(L)I]_n$ chains [L = pyridine,[21] 4-methylpyridine, 2,4-dimethylpyridine and 3,4-dimethylpyridine,[12] identified in the CSD by KALPAO, YUXTIV, YUXTHU and YUXVET Refcodes, respectively]. All these structures show short Ag···Ag distances (ranging from 3.006 to 3.164 Å). Main crystallographic data and selected bond distances and angles for all compounds are reported in Tables S1–S4.

Photophysical behavior

Crystals of **1-Ag** at 298 K display a quite complex emissive behavior comprising fast and long lived components (overall quantum efficiency, Φ, equal to 19%) with relative intensities varying according to the excitation energy and covering a large portion (from 385 to 700 nm) of the visible spectrum (see Figure 2 and Table 1).

In particular, a very weak high energy band with peaks at about 385 and 400 nm, recognizable as a fluorescent emission by its lifetime in the ns regime (τ = 2,15 ns, see Figure S1), is present together with three sets of vibrationally resolved long lived components by exciting at $\lambda_{exc} \geq 340$ nm: a well separated high energy phosphorescence, HEP (411, 445 nm), together with two partially overlaid phosphorescences at lower energy (medium energy phosphorescence, MEP at 446, 476 and 509 nm, and low energy phosphorescence LEP at 494, 530, 575, 620 and 680 nm,

View Article Online
DOI: 10.1039/D0QI01277C

τ_{av} = 39.76 ms, see Figure S2). Analysis of emission and excitation spectra suggests that LEP is the dominant deactivation channel when crystals are excited in the 350-370 nm range, while the MEP is intensified by exciting at 340 nm. Finally, HEP becomes visible and is gradually intensified on moving from 390 to 397 nm excitation. Of the three sets of bands present in the excitation spectra, recognizable by vibrational peaks at 343 and 363 nm; 355 and 375 nm and at 397 nm, the first two bands may correspond, respectively, to the first excited singlet states, $^1ES_2$ and $^1ES_1$, while the latter one may be associated to $^3ET_1$. Thus, excitation to $^1ES_1$, besides fluorescence, results primarily in LEP emission; population of $^1ES_2$ results in MEP together with LEP, while HEP is easily activated by directly populating $^3ET_1$. It has, however, to be mentioned the presence of a very weak absorption peak at about 428 nm when monitoring the lowest emission peaks (see Figure 2), whose origin could be ascribed to supramolecular interactions.

MEP and LEP are visible in time delayed spectra regardless the excitation wavelength (corresponding to $^3ET_1$, at 397 nm, or to $^1ES_1$, at 360 nm; see Figure 2), revealing that ISC from S_1 is a possible mechanism to populate the triplet states corresponding to the two long lived emissions. HEP is hardly visible in the time delayed spectra, probably due to its short lifetime, close to the instrument temporal resolution (50 μs).

Figures S3-S6). In particular, a weak fluorescence at 386 and 395 nm is visible together with HEP at 425 and 446 nm, MEP at 440, 470 and 506 nm and LEP at 490, 528, 576, 631 and 701 nm. Again, emissions' relative intensities are affected by the excitation wavelength. All components are visible in the spectrum at λ_{exc} =350 nm; MEP is intensified by 340 nm excitation and HEP is selectively activated by exciting in the 390-397 nm range.

Comparison of excitation spectra at 298 and 77 K (Figure 2 and 3) shows that vibrational peaks assigned to $^1ES_1$ (355 and 375 nm) at 298 K, are still present and very well resolved at low temperature (336, 353 and 376 nm) when monitoring the LEP. $^3ET_1$ at 397 nm is still present but hardly visible at 77 K, in correspondence of the HEP. However, other peaks at high energy (wavelength shorter than 305 nm) are present at 77 K but absent in the 298 K excitation profiles. By exciting at these high energies (300 nm), a broad band covering the 380-700 nm region appears in the emission spectrum (see Figure S7). The broad shape of this band could be originated from the convolution of vibrational peaks belonging to the various electronic components which seem to be simultaneously activated at high energy. It is plausible that these high energy excitations are easily deactivated by non radiative transitions at 298 K.

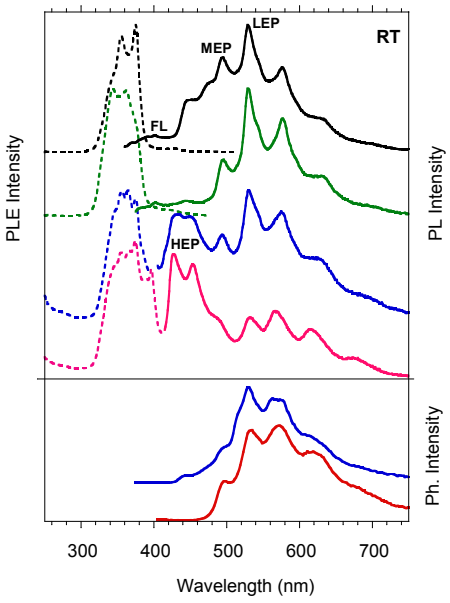

Figure 2. Normalized emission and excitation spectra of crystals of **1-Ag** at 298 K. Upper panel: PL spectra (solid line) at λ_{exc} = 397 nm (pink line); 390 nm (blue line); 355 nm (green line); 341 nm (black line) and PLE spectra (dotted line) at λ_{em} = 410 nm (blue line); 430 nm (pink line); 495 nm (green line); 530 nm (black line). Lower panel: phosphorescence spectra (blue line, delay 200 μs, window 500 μs, λ_{exc} = 360 nm; red line, delay 100 μs, window 500 μs, λ_{exc} = 397 nm). All the spectra are vertically shifted for clarity.

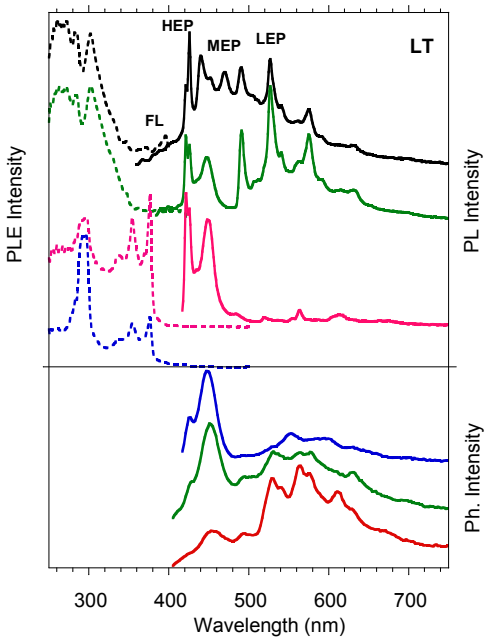

Figure 3. Normalized emission and excitation spectra of crystals of **1-Ag** at 77 K. Upper panel: PL spectra (solid line) at λ_{exc} = 397 nm (pink line); 364 nm (green line); 340 nm (black line), and PLE spectra (dotted line) at λ_{em} = 421 nm (black line); 443 nm (green line); 527 nm (pink line); 630 nm (blue line). Lower panel: phosphorescence spectra (λ_{exc} = 397 nm; blue line, delay 50 μs, window 100 μs; green line, delay 100 μs, window 500 μs; red line, delay 1 ms, window 5ms). All the spectra are vertically shifted for clarity.

To get deeper insight in **1-Ag** photophysics, measurements at 77 K were performed (see Figure 3). The four emissions observed at 298 K are still present though with higher vibrational resolution and longer lifetimes (see Table 1 and

In delayed spectra (Bottom of Figure 3), HEP contribution is well visible thanks to its increased lifetime with respect to 298 K, while the evolution of the spectral shape, observed by recording

View Article Online
DOI: 10.1039/D0QI01272E

the emission at different delays, evidences that emission lifetimes increase in the order HEP<MEP<LEP.

Based on crystallographic results, it is evident that ligand's H-aggregation, present in the free **TT** itself, is preserved in the Ag(I) coordination polymer **1-Ag**. This packing motif of the organic component has already been recognized as responsible for the long lived, low energy emission of many members of the **TT**-family.[18,22] In particular, **1-Ag** LEP peaks show a remarkable similarity with the vibrational components of the T_H-S_0 emission of the mono-iodinated (**TTI**) and the co-crystal of **TT** with 1,4-diiodiotetrafluorobenzene (**TTCo**) derivatives at 77 K (see Table 1 and Figure S8).[22c] This observation is in agreement with the comparable interplanar distance of **TT** units in the three compounds (3.173 Å in **1-Ag,** 3.309 Å in **TTI** and 3.332, 3.488 Å in **TTCo**). Therefore, it is reasonable to assign LEP to deactivation from T_H. Impressively, close inspection of the 77 K emission spectra of **1-Ag**, **TTI** and **TTCo**, reveals the same pattern for the MEP of the former with emission from T_I of the two latter (see Table 1). Such phosphorescence was previously ascribed to the I···N halogen bonding interaction which is present in the structures of **TTI** and **TTCo**, but absent in **1-Ag**. We cannot ignore, however, that the similarity in position and shape of the emissions of the three systems, all containing **TT** and I atoms, is too strong to be considered a coincidence. It is therefore possible a common origin (T_I-S_0) with a mechanism different from the one previously suggested. Looking at the shorter contacts between adjacent stairs (in **1-Ag**), helices (in **TTI**) and chains (in **TTCo**) involving I atom, it is found that the three structures share a comparable I···C distance of 3.664, 3.764 and 3.736 Å. Although these contacts cannot be interpreted as halogen bonding because the relative orientation of the interacting moieties is far from the T-shaped one,[23] they are compatible with intermolecular electronic coupling of two units with partial orbital overlapping.[20] To point at the common origin, involving I atom, MEP emission in **1-Ag** is indicated as a T_I-S_0 deactivation.

Finally, HEP, in agreement with previous findings[22d,22e] and theoretical calculations (see below), seems to be due to deactivation from a ligand centered triplet state (T_M-S_0, where M stands for "molecular" in order to distinguish its origin from the LEP and MEP supramolecular one) as suggested also by the observation that it is magnified by directly populating $^3ET_1$. The ligand centered nature of the T_M-S_0 emission is further supported by the energy spacing (about 1300-1550 cm^{-1}) of its vibrational components which can be associated to a vibronic progression involving imidazole ring modes.[24] Similar values are calculated for the vibrational peaks of MEP and LEP, having themselves a negligible contribution from the metal.

This **1-Ag** rich photophysics was to us worth to be compared with that of the isostructural Cu(I) derivative $[Cu(TT)I]_n$, **1-Cu**, for which we have recently reported a quite simple emissive behavior comprising only one broad emission of ^{3}MLCT character at 568 nm (Φ =18%).[17] In view of the results obtained for **1-Ag**, and especially due to the presence of the H-aggregates LEP emission in the spectrum of this latter compound, we decided to deepen our study on the photophysics of **1-Cu** (see Figure 4 and Table 1). By this further investigation, we found that by exciting in the 300-360 nm region, the spectrum of the compound is, in fact, dominated by the quite intense ^{3}MLCT (T_M-S_0) phosphorescence (568 nm; 31 μs see ref. [17]). However, with lower excitation energy (λ_{exc} >390 nm) two far less intense vibronically resolved long lived emissions are observed (see upper panel of Figure 3). In particular, a lower energy and longer lived (302 μs, see Figure S9) component, LEP, with peaks at 536, 582, 623 nm, impressively overlapped with that of the **1-Ag** analog (the two compounds sharing an identical interplanar **TT** distance equal to 3.173 Å) and a higher energy phosphorescence with peaks at 431, 460 and 487 nm, are collected for **1-Cu** at 298 K. This latter component lies in-between HEP and MEP recorded for the **1-Ag** analog. However, since experiments at 77 K (see later) reveal its close similarity with **1-Ag** MEP and since the I···C interstep distance, 3.721 Å, is compatible with intermolecular electronic coupling (extrinsic heavy-atom effect), it is reasonable to use the same acronym (MEP, T_I-S_0 emission) to refer also to it. It is worth noting that the shorter I···C distance of **1-Ag**, 3.664 Å, might justify its MEP lower energy. The delayed spectrum displays, at room temperature, only the longer lived LEP (Bottom of Figure 4).

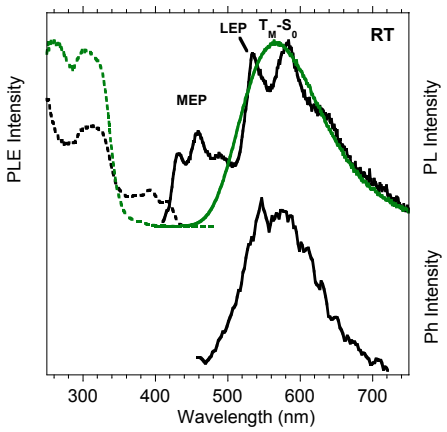

Figure 4. Normalized emission and excitation spectra of crystals of **1-Cu** at 298 K. Upper panel: PL spectra (solid line) at λ_{exc} = 300 nm (green line); 390 nm (black line) and PLE spectra (dotted line) at λ_{em} = 460 nm (black line); 563 nm (green line). Lower panel: phosphorescence spectrum (λ_{exc} = 420 nm; black line, delay 100 μs, window 500 μs).

By analyzing the excitation spectra of **1-Cu** (see Figure 4), two sets of bands are clearly visible at low energy, peaked at about 309 and 397, 420 nm, that may be tentatively described as ^1ES_n (309 nm) and $^3ET_1$ (397, 420 nm), respectively. Based on the excitation spectrum measured at 77K (see Figure 5), the presence of an additional peak (370 nm) in between ^1ES_n (310 nm) and $^3ET_1$ (391, 415nm) cannot be excluded. According to this assignment, excitation to ^1ES_n or $^1ES_1$ selectively results in the broad 568 nm ^{3}MLCT emission, while $^3ET_1$ activates the MEP and LEP resolved phosphorescences.

The similarity of LEP for **1-Cu**, **1-Ag**, **TTI** and **TTCo** (see Figure S8), supports its ligand's H-aggregation origin (T_H-S_0) also for the copper derivative. Comparing the two isostructural **1-Cu** and **1-Ag**, it is clear that the metal plays on LEP a secondary role and can be therefore referred to as an "external" perturber.[25] The same can be observed for MEP of the two compounds, in

View Article Online
DOI: 10.1039/D0QI01377C

agreement with its I···C intermolecular electronic coupling origin. Again, this metal secondary effect results in shorter emission lifetimes for MEP and LEP of Cu(I) having a lower atomic number (see Table 1).

Emission spectra collected at 77 K (see Figure 5, Table 1 and Figures S10-S11), still show the presence of the broad 568 nm long lived band of MLCT character when exciting at high energy (300-340 nm) together with the structured LEP and MEP (better isolated when exciting to $^3ET_1$, 390-420 nm). In the time delayed spectra, the MEP component is now observed overlapped to the LEP profile displaying narrow peaks whose relative intensity varies with the delay time. The perfect agreement between Ag and Cu LEP and MEP (see Table 1) supports their common origins. It is to be pointed out that a weak fluorescent component (at 415 and 430 nm) cannot be excluded.

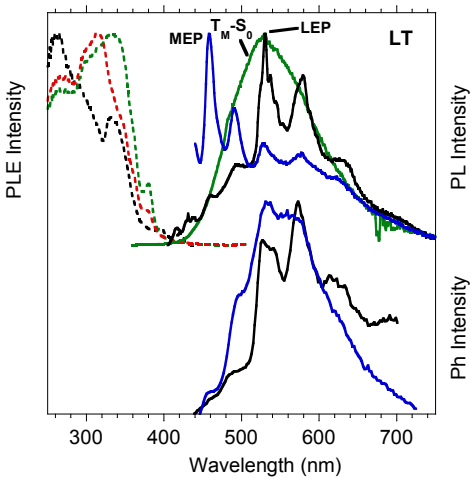

Figure 5. Normalized emission and excitation spectra of crystals of **1-Cu** at 77 K. Upper panel: PL spectra (solid line) at λ_{exc} = 340 nm (green line); 390 nm (black line); 420 nm (blue line) and PLE spectra (dotted line) at λ_{em} = 460 nm (black line); 530 nm (green line) and 633 nm (red line). Lower panel: phosphorescence spectra (λ_{exc} = 420 nm; blue line, delay 100 μs, window 500 μs; black line, delay 1 ms, window 5ms).

The main experimental results obtained for **1-Cu** and **1-Ag** can, therefore, be summarized as follow: at intramolecular level, for **1-Cu** the dominant deactivation channel, when exciting at high energy, is from a ^{3}MLCT triplet populated through ISC from singlet manifolds. This channel is absent in the case of **1-Ag** for which a fluorescence and a ligand centered phosphorescence (HEP) are observed. At supramolecular level, MEP and LEP are present for both compounds.

To confirm the origin of the intramolecular emission bands in **1-Ag** and **1-Cu**, DFT and TDDFT calculations have been performed on the $[M(TT)I]_4$ model compounds (M=Ag, Cu). It should be noted that geometry optimization of discrete models implies a loss of the symmetry characterizing the $[M(TT)I]_n$ polymeric structure owing to major boundary effects. This may reflect into artificial splitting of the electronic excitation levels, so that a close one-to-one correspondence between computed and observed states is not allowed. The first singlet level (S_1, see Figures S22-S25 and Table S6, S7), computed at 274 (Ag) and 307 nm (Cu), has ^{1}XMCT character with some ^{1}XMLCT contribution, much greater for the Cu compound with respect to the Ag one.

In agreement, a Quantum Theory of Atoms in Molecules (QTAIM) analysis[26] (see Table S5 and Figure S21) shows higher shared-shell character for the Cu–N bond with respect to the Ag–N one, as indicated in particular by the larger value of Delocalization Index, i.e., the average number of electrons shared between M and N (0.452 vs. 0.368 for the Cu–N and the Ag–N bond, respectively). This result could explain the greater metal contribution on the intramolecular emissive behavior of **1-Cu**. In particular, the suppression of fluorescence through easy ISC to close triplets, the shorter lifetimes and the importance of the MLCT emission.

To further analyze the compounds' intramolecular deactivation channels, DFT/TDDFT calculations provide the first triplet levels (T_1÷T_4 and T_1÷T_3 for Ag and Cu compounds, respectively) at 324 (Ag) and 329 nm (Cu), with mixed ^{3}LC/^{3}XMLCT character. In addition, a low energy ^{3}XMCT/^{3}XMLCT triplet state (T_4, at about 0.01 eV from T_1÷T_3) is calculated for Cu but it is absent in the Ag model compound. For this latter, pure ^{3}XMCT triplet states are computed at higher energy (T_9, T_{14}), lacking close singlet state which could allow their population by ISC.

Therefore, it is possible that the observed **1-Ag** HEP emission can be accessed either through triplet direct population at low energy or through ISC from S_1. The latter process being facilitated by the presence of triplet states (T_{15} and T_{16}) close to S_1 and having partial σ character deriving from the coordinating nitrogen atoms.

On the other side, the unresolved low energy phosphorescence observed at 568 nm for **1-Cu** when exciting at high energy (about 300 nm) may be ascribed to emission from T_4, which could relax to lower energy than that of T_1÷T_3 states. T_4 can be either accessed by IC from higher triplet states having the same character, that are populated by ISC from close high energy singlet states or by ISC from S_1.

Finally, the different nature of the M–N bond may also explain the stronger metal (Cu) contribution in both supramolecular MEP and LEP emissions, manifesting into the shorter lifetimes observed for **1-Cu** with respect to **1-Ag** in disagreement with the expected heavy atom effect, a result already observed for some isostructural Cu and Ag complexes.[7]

Transitions involved in the photophysical behavior of **1-Ag** and **1-Cu** are exemplified in Figure 6.

Surprisingly, calculations on the $[Ag(TT)I]_4$ model do not provide any transition of Cluster Centered (CC) character, as should be expected according to the Ag···Ag distance, 3.1591(5) Å, significantly shorter (8.2%) than two times the Ag van der Waals radius, 3.44 Å. Such result should be related to the QTAIM analysis previously reported on the Ag_2I_2 core,[27] where the intermetallic distance was systematically varied by 0.1 Å in order to establish the threshold for the presence of the Ag···Ag bond critical point, bcp, denoting the presence of argentophilic interaction.[28] According to this analysis, such threshold lies in the 3.21-3.31 Å range, somewhat shorter than 3.44 Å owing to the presence of the electronegative iodides. Interestingly, QTAIM analysis on $[Ag(TT)I]_4$ model, displaying intermetallic distances equal to 3.19 and 3.24 Å, does not provide any bcp

along the Ag···Ag interatomic line. This result suggests a role of the ligand in further depleting the electron density distribution around the metal center, in addition to the effect exerted by the iodide ions. A CC contribution to the photophysical behavior of **1-Cu** is, of course, to be excluded based on the Cu···Cu distance (3.2479 (7) Å) much larger than two times the Cu vdW radius (2.80 Å).

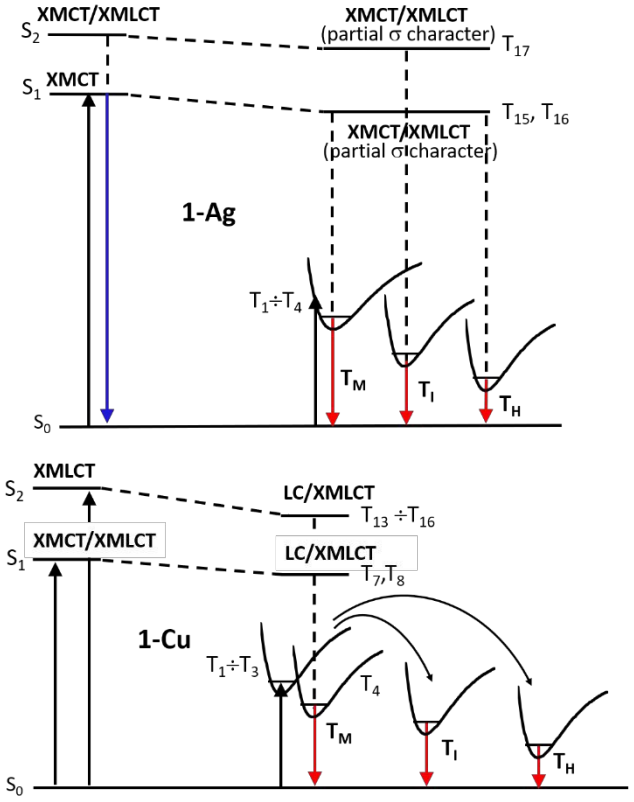

Figure 6. Schematic photophysical processes of **1-Ag** (top) and **1-Cu** (bottom) (fluorescence and phosphorescence shown as blue and red arrows, respectively).

3D Coordination Polymer [Ag(TT)Cl]$_n$ (2-Ag)

Crystals of the coordination polymer 3D [Ag(TT)Cl]$_n$ (**2-Ag**) have been obtained by solvothermal reaction of AgCl and **TT** in CH_3CN/DMF at 120 °C for 36 h. The compound crystallizes in the cubic space group *Pa*–3. The asymmetric unit contains one silver atom, one chloride ion and one third of a **TT** ligand, with the silver and chlorine atoms and the centroid of the **TT** molecule residing on a three-fold rotation axis (Figure 7). The structure is isostructural to [Cu(TT)Cl]$_n$ [17] and, similarly, shows the same 3D coordination network.[17] Unlike **1-Ag**, in this structure the **TT** ligand uses the nitrogen atoms of all of its three imidazole moieties to interact with silver atoms, adopting a μ_3-bridging coordination mode. Silver atoms are in an AgN_3Cl distorted tetrahedral environment, coordinating three different μ_3-bridging **TT** ligands and one terminal chloride anion [Ag–N = 2.3544(10); Ag–Cl = 2.4562(5) Å]. As a result, a 3-connected 3D network of chiral **srs** topology is obtained,[29] in which the 3-connected nodes are both the silver atoms and the **TT** centroids.

View Article Online
DOI: 10.1039/D0QI01377C

Furthermore, the structure is 2-fold interpenetrated, so that two single chiral networks give a centrosymmetric framework through a centre of inversion. **TT** ligands belonging to different **srs** networks are involved in stacking interactions characterized by a distance between the parallel mean planes of 3.3281(4) Å and a distance between the centroid of the triazine moieties of 3.2797(6) Å. These values are very similar to those found for **2-Cu**, namely 3.3135(3) and 3.2892(15) Å, respectively.

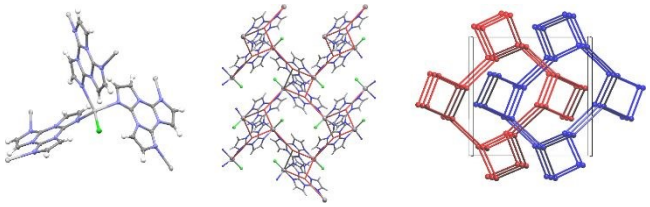

Figure 7. Views of the crystal structure of **2-Ag** showing the coordination environment around the silver atoms (left), a single 3D network superimposed with the simplified srs net (in magenta) along the a direction (middle), and the two interpenetrated simplified srs nets of opposite chirality (in red and blue) along the crystallographic c direction (right). Ellipsoids are drawn at 50% probability.

Photophysical behavior

Crystals of **2-Ag** display at 298 K an excitation dependent steady state emission spectrum (see upper panel of Figure 8). In particular, a fluorescent broad band at 448 nm (τ_{av} = 4.45 ns, see Table 1) appears by exciting at 360 nm and a broad unresolved band at 505 nm by exciting at 440 nm. Time resolved emission spectra at 298 K allow to recognize the presence of two long lived superimposed emissions: one broad with shorter lifetimes and one vibrationally resolved (526, 565 and 615 nm) longer lived (47.7 ms, see Figure S12) component (see lower panel of Figure 6). The latter, due to its similarity with the LEP of **1-Ag** and **1-Cu** and in agreement with single crystal XRD study, can be ascribed to the presence of **TT** H-dimers in **2-Ag** crystal structure.

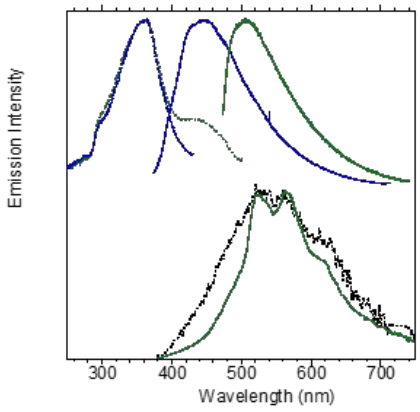

Figure 8. Normalized emission and excitation spectra of crystals of **2-Ag** at 298 K. Upper panel: PL spectra (solid line) at λ_{exc} = 360 nm (blue line); 440 nm (green line) and PLE spectra (dotted line) at λ_{em} = 450 nm (blue line); 520 nm (green line). Lower panel: phosphorescence spectrum (λ_{exc} = 360 nm; black dotted line, delay 200 μs, window 500 μs; solid green line, delay 5ms, window 20ms).

View Article Online
DOI: 10.1039/D0QI01377C

Again, based on this results, we decided to deeper investigate the photophysics of the isostructural Cu(I) analog, **2-Cu**, which we previously reported possessing only one major broad band of ^{3}MLCT character (Φ equal to 4%).[17] Differently from **1-M** and **2-Ag**, the steady state emission spectrum of **2-Cu** is not affected by the excitation wavelength and only one broad emission at 570 nm is present (see upper panel of Figure 9). However, two long lived components at 515 (τ_{av} = 6.24 μs, see ref. [17]) and 560 nm (τ_{av} = 3.56 ms, see Figure S13) are present, as suggested by time resolved spectroscopy (see lower panel of Figure 9 and Table 1). The presence of a second phosphorescent component, although lacking the vibronic progression of the other compounds of this family, is probably to be correlated with the formation of ligand's H dimers inside the structure.

The high energy component has, on the other side, to be correlated to a triplet state of intramolecular origin (T_M, see discussion below). It is interesting to point out that also for the **2-M** derivatives, as already highlighted for the **1-M** ones, a reduced heavy metal effect is observed for Ag with respect to Cu. For the former, in fact, not only longer phosphorescence lifetimes are measured but also emission from S_1, resulting in a fluorescent peak in the emission spectrum of both Ag compounds, becomes competitive with ISC to triplet states.

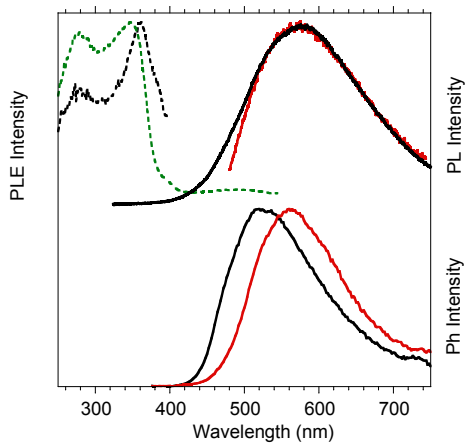

Figure 9. Normalized emission and excitation spectra of crystals of **2-Cu** at 298 K. Upper panel: PL spectra (solid line) at λ_{exc} = 300 nm (black line); 460 nm (red line) and PLE spectra (dotted line) at λ_{em} = 410 nm (black line); 578 nm (green line). Lower panel: phosphorescence spectrum, λ_{exc} = 360 nm (black line, delay 100 μs, window 200 μs; red line, delay 5 ms, window 50 ms).

DFT/TDDFT calculations on the $M(TT)_3Cl$ models provide a rather similar picture of the electronic levels for the two compounds (see Figures S27-S29 and Tables S8, S9). In both cases, lower energy triplet states with mixed ^{3}LC/^{3}XMLCT character are determined. As found for **1-Ag**, and differently from **1-Cu**, these states can be accessed either through triplet direct population at low energy or through ISC from computed $S_1 \div S_3$ to close triplet states ($T_{16} \div T_{18}$ for $Ag(TT)_3Cl$ and $T_{13} \div T_{15}$ for $Cu(TT)_3Cl$). The latter process is facilitated by partial σ character of $S_1 \div S_3$ states deriving from the coordinating nitrogen atoms.

Transitions involved in the photophysical behavior of **2-Ag** and **2-Cu** are exemplified in Figure 10.

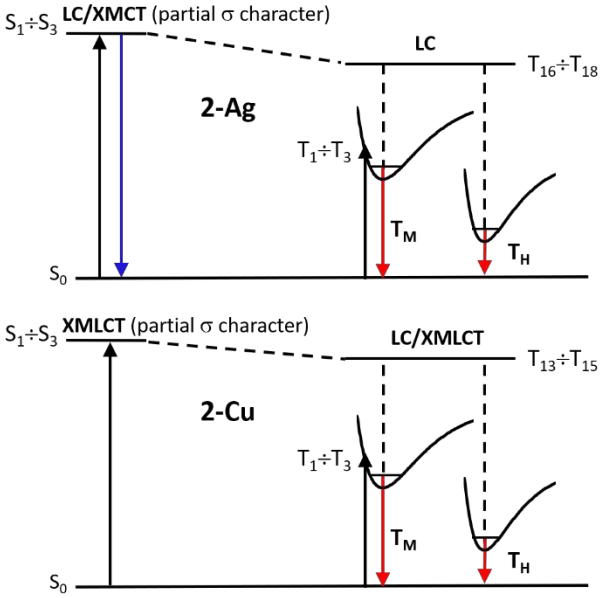

Figure 10. Schematic photophysical processes of **2-Ag** (top) and **2-Cu** (bottom) (fluorescence and phosphorescence shown as blue and red arrows, respectively).

3D Coordination Polymer $[Ag_3(TT)_4]_n(NO_3)_{3n}\cdot 6nH_2O$ (3-Ag)

Microcrystalline powders of the coordination polymer 3D $[Ag_3(TT)_4]_n(NO_3)_{3n}\cdot 6nH_2O$ (**3-Ag**) have been obtained by mixing an ethanolic solution of $AgNO_3$ into a dichloromethane solution of **TT**. After filtration, the resulting clear solution was slowly evaporated to give crystals suitable for X-ray analysis. Crystals of **3-Ag** can also be prepared by slow diffusion of an ethanolic solution of $AgNO_3$ into a solution of **TT** in dichloromethane (see ESI). The compound crystallizes in the cubic space group *I*–43*d*. The asymmetric unit contains one silver atom lying on a 4-fold rotoinversion axis, one third of a **TT** ligand whose centroid is located on a 3-fold rotation axis, a nitrate anion disordered around a 3-fold axis, and a disordered water molecule located on a 2-fold rotation axis (Figure 11). The silver atoms are coordinated to four **TT** molecules in a distorted tetrahedral environment (tetragonal disphenoid) with a bond distance Ag–N = 2.308(4) Å and bond angles N–Ag–N = 2 × 124.7(2) and 4 × 102.45(9)°. As in the case of **2-Ag**, **TT** molecules adopt a μ_3-bridging coordination mode using the nitrogen atoms of all of its three imidazole moieties to interact with silver atoms. As a consequence, a binodal (3,4)-connected 3D coordination network of **ctn** topology[29] [Point Symbol $(8^3)_4(8^6)_3$] is formed, in which the silver atoms are the 4-connected nodes and the **TT** molecules the 3-connected ones. Unlike **1-Ag** and **2-Ag**, no stacking interactions between **TT** molecules are present in **3-Ag**, as well as other type of non-bonded interactions. Nitrate anions and water molecules are disordered and located in the void space of the 3D structure. They are involved in hydrogen bonds generating a supramolecular network in the cavity of the coordination network.

View Article Online
DOI: 10.1039/D0QI01377C

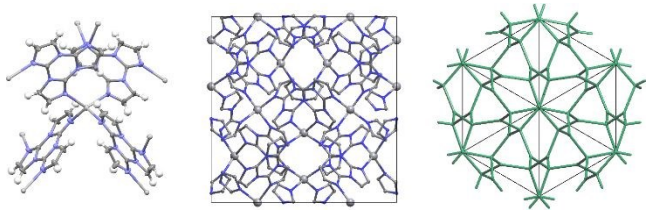

Figure 11. Views of the crystal structure of **3-Ag** showing the coordination environment around the silver atoms (left), the single 3D coordination network along the crystallographic a direction (middle), and the simplified (3,4)-connected net of ctn topology along the [1 1 1] direction (right). Water molecules and nitrate anions are omitted for clarity. Ellipsoids are drawn at 50% probability.

Photophysical behavior

The steady state spectrum of crystals of **3-Ag** at 298 K (Φ equal to 7.5%) displays excitation dependent emissions (see upper panel of Figure 12). In particular, a broad fluorescent band at 404 nm (τ_{av} = 1.49 ns) is observed with 300 nm excitation, one phosphorescence at 454 nm (τ_{av} = 3.41 ms) with 405 nm excitation and a second long lived (τ_{av} = 1.04 ms) component at 556 nm with 500 nm excitation (see Figure S14-S15 and Table 1). The two phosphorescences can be isolated through time resolved spectroscopy exciting at 300 nm (see lower panel of Figure 12). Looking at the excitation spectrum, the highest peak (at 340 nm) should be associated with the first excited singlet state, $^1ES_1$, while its shoulder at higher energy (at about 300 nm) may correspond to $^1ES_2$. The lower energy bands, centered at about 400 and 460 nm, more evident at low temperature (see Figure S16), may be related to triplet states of different nature, ^3ET_n and $^3ET_1$, respectively, which reflect into the anti-Kasha behavior of this compound able to emit also from a high energy triplet state. It should be noted that, differently from **1-M** and **2-M**, **3-Ag** lacks H-aggregation of the ligands inside its crystal structure, so that both observed phosphorescences must be originated from molecular entities. DFT/TDDFT calculations on the $Ag(TT)_4^+$ discrete model (see Figures S30, S31 and Table S10) reveal that, differently from **1-Ag** and **2-Ag**, all the low energy transitions involve molecular orbitals (MOs) localized on the ligand, with only a minor contribution of the metal ion in the first unoccupied orbitals. In particular, the lower singlet and triplet states, $S_1 \div S_4$ and $T_1 \div T_4$, computed at 234 and 330 nm and corresponding to $^1ES_1$ and $^3ET_1$, respectively, have mainly LLCT and, in a lesser extent, ILCT character. More precisely, close inspection of the MOs' populations shows that these transitions involve charge transfer from two **TT** units of $Ag(TT)_4^+$ to the other two (LLCT transitions), or from two **TT** units to the same ones (ILCT transitions). Only at higher energy, another set of singlet and triplet levels ($S_{13} \div S_{16}$ and $T_9 \div T_{12}$, computed at 205 and 295 nm, respectively) is found, where also inner occupied MOs, having a partial delocalization on the metal, contribute to the transitions. The different composition of the $T_1 \div T_4$ and $T_9 \div T_{12}$ sets of levels may explain the observed phosphorescence from $^3ET_1$ and ^3ET_n, respectively. Access to these levels may take place by their direct population or through ISC from close singlet manifolds having the proper MOs' populations.

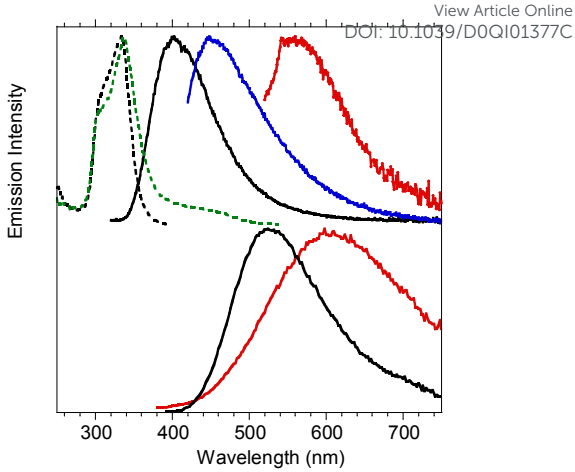

Figure 12. Normalized emission and excitation spectra of crystals of **3-Ag** at 298 K. Upper panel: PL spectra (solid line) at λ_{exc} = 300 nm (black line); 405 nm (blue line); 500 nm (red line) and PLE spectra (dotted line) at λ_{em} = 410 nm (black line); 566 nm (green line). Lower panel: phosphorescence spectrum, λ_{exc} = 300 nm (red line, delay 50 μs, window 100 μs; black line, delay 2 ms, window 10 ms).

Figure 13 shows a picture of the transitions involved in the photophysical behavior of **3-Ag**, based on DFT/TDDFT calculations. The proposed mechanism seems the only reasonable to support the observed phosphorescent anti-Kasha behavior. However, it appears not consistent with the experimental observation that both phosphorescences are activated by excitation to S_1 and that the two display comparable lifetimes despite a greater metal contribution in the higher energy component. Although, it should be noted that, as observed for **1-Ag** and **2-Ag**, the Ag contribution on lifetimes is only marginal.

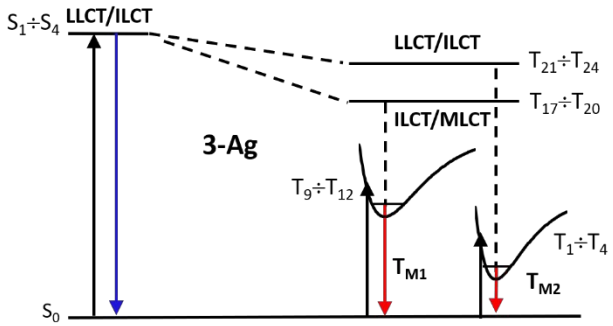

Figure 13. Schematic photophysical processes of **3-Ag** (fluorescence and phosphorescence shown as blue and red arrows, respectively).

View Article Online
DOI: 10.1039/D0QI01377C

Table 1. Photoluminescence data at 298 and 77K. Values for TT, TTI and TTCo are taken from refs. [18] and [22c].

Sample	298 K				77 K		
	Φ (%)	λ_{em} (nm)	τ	Emission origin	λ_{em} (nm)	τ	Emission origin
TT (cryst)	30	400	7.67 ns	S_1-S_0	403	8.96 ns	S_1-S_0
		525	970 ms	T_H-S_0	510	1.075 s	T_H-S_0
TTI (cryst)	<0.1	456	1.36 ns	S_1-S_0	458	2.76 ns	S_1-S_0
					460, 495, 530	14.17 ms	T_I-S_0
		517, 563, 612	63.99 ms	T_H-S_0	511,526,558 573,610	23.35 ms	T_H-S_0
		630	0.53 µs	T_M-S_0	640	23.66 µs	T_M-S_0
TTCo (cryst)	5	410	2.56 ns	S_1-S_0	440	3.42 ns	S_1-S_0
					463,497,537	13.92 ms	T_I-S_0
		496, 528, 566	21.43 ms	T_H-S_0	490,527,560	20.14 ms	T_H-S_0
					720	6.83 µs	T_M-S_0
1-Ag (cryst)	19	385, 400	2.15 ns[a]	S_1-S_0	386, 395	2.31 ns[c]	S_1-S_0
		411, 445	< 50 µs	T_M-S_0	425, 446	421.03 µs[d]	T_M-S_0
		446, 476, 509	2.84 ms[d]	T_I-S_0	440, 470, 506, 541	5.67 ms[e]	T_I-S_0
		494, 530, 575, 620, 680	39.76 ms[b]	T_H-S_0	490, 528, 576, 631, 701	44.51 ms[f]	T_H-S_0
1-Cu (cryst)	18	568	32 µs[17]	T_M-S_0	568	47.14 µs[17]	T_M-S_0
		431, 460, 487		T_I-S_0	430, 460, 494, 538	41.85 µs[h]	T_I-S_0
		536, 582, 623	302.12 µs[g]	T_H-S_0	529, 580, 627	1.030 ms[g]	T_H-S_0
2-Ag (cryst)		448	4.45 ns	S_1-S_0			
		520		T_M-S_0			
		526, 565, 615	47.7 ms[i]	T_H-S_0			
2-Cu (cryst)	4	515	6.24 µs[17]	T_M-S_0			
		560	3.56 ms[l]	T_H-S_0			
3-Ag (cryst)	7.5	404	1.49 ns[m]	S_1-S_0	391	1.76 ns[p]	S_1-S_0
		454	3.41 ms[n]	T_{M1}-S_0	471	32.69 ms[q]	T_{M1}-S_0
		556	1.04 ms[o]	T_{M2}-S_0	565	33.36 ms[r]	T_{M2}-S_0

[a]λ_{em} = 400 nm λ_{exc} = 374 nm; [b]λ_{em} = 530 nm λ_{exc} = 374 nm; [c]λ_{em} = 424 nm λ_{exc} = 374 nm; [d]λ_{em} = 449 nm λ_{exc} = 374 nm; [e]λ_{em} = 449 nm λ_{exc} = 360 nm; [f]λ_{em} = 530 nm λ_{exc} = 374 nm; [g]λ_{em} = 530 nm λ_{exc} = 390 nm; [h]λ_{em} = 550 nm λ_{exc} = 300 nm; [i]λ_{em} = 566 nm λ_{exc} = 360 nm; [l]λ_{em} = 570 nm λ_{exc} = 360 nm; [m]λ_{em} = 410 nm λ_{exc} = 300 nm; [n]λ_{em} = 520 nm λ_{exc} = 300 nm; [o]λ_{em} = 650 nm λ_{exc} = 300 nm; [p]λ_{em} = 392 nm λ_{exc} = 300 nm; [q]λ_{em} = 448 nm λ_{exc} = 334 nm; [r]λ_{em} = 563 nm λ_{exc} = 334 nm.

Conclusions

The versatility of cyclic triimidazole in assembling coordination polymers is here extended to the preparation and structural characterization of three new Ag(I) compounds, i.e. one 1D double-stranded stair (**1-Ag**) and two 3D networks (**2-Ag** and **3-Ag**). Remarkably, the **TT** H-aggregation motif, present in **1-Ag** and **2-Ag**, as well as in most **TT** derivatives,[17,22] is disrupted in **3-Ag**.

A detailed photophysical study on the three Ag(I) compounds and the isostructural **1-Cu** and **2-Cu** derivatives, complemented by DFT/TDDFT calculations, has allowed to shed light, for the first time, to new interesting aspects concerning their emissive behavior. All the investigated compounds show excitation wavelength-dependent photoluminescence, including, for Ag(I) derivatives, fluorescence and long-lasting phosphorescence. For Ag(I) compounds the decay paths, mostly of Ligand-Centered nature, are simultaneously activated but varied in intensity by changing the excitation energy. On the contrary, Cu(I) compounds show non-thermally equilibrated XMLCT and Ligand-Centered emissive states. The different nature of the emissive states of Ag(I) and Cu(I) compounds is explained by larger shell-shared character of the Cu–N bond with respect to the Ag–N one, on the basis of QTAIM topological analysis of electron density.

Differently from what generally reported, the Ag(I) compounds here investigated are as emissive as the Cu(I) analogues. Particularly significant are the results concerning the double-stranded stair CPs which display almost overlapped spectra relative to the bands associated with H-aggregates of the ligand (LEP) and intermolecular electronic coupling by extrinsic heavy-atom effect (MEP). No argentophilic interaction is detected in this structure, in spite of the quite short Ag···Ag interatomic distance, 3.1591(5) Å. Interestingly, the distinctive signature of the structured LEP is absent in **3-Ag**, confirming unambiguously the assignment of this band to the presence of **TT** H-aggregates.

In addition to the progress obtained in clarifying the mechanism involved in the photophysical behavior of Ag(I) and Cu(I) CPs, this investigation further supports **TT** as a useful scaffold to build up new solid-state materials with tunable emissions for bioimaging, sensors, security, OLEDs, optical storage and many other applications.

Conflicts of interest

There are no conflicts to declare.

Acknowledgements

The use of instrumentation purchased through the Regione Lombardia-Fondazione Cariplo joint SmartMatLab Project is gratefully acknowledged. The authors thank Arianna Civiletti for some experimental work.

Notes and references

View Article Online
DOI: 10.1039/D0QI01377C

1 (a) A. Kobayashi and M. Kato, Stimuli-responsive Luminescent Copper(I) Complexes for Intelligent Emissive Devices, *Chem. Lett.*, 2017, **46**, 154-162. (b) R. Czerwieniec, M. J. Leitl, H. H. H. Homeier and H. Yersin, Cu(I) complexes – Thermally activated delayed fluorescence. Photophysical approach and material design, *Coord. Chem. Rev.*, 2016, **325**, 2-28. (c) E. Cariati, E. Lucenti, C. Botta, U. Giovanella, D. Marinotto and S. Righetto, Cu(I) hybrid inorganic–organic materials with intriguing stimuli responsive and optoelectronic properties, *Coord. Chem. Rev.*, 2016, **306**, 566-614. (d) K. Tsuge, Y. Chishina, H. Hashiguchi, Y. Sasaki, M. Kato, S. Ishizaka and N. Kitamura, Luminescent copper(I) complexes with halogenido-bridged dimeric core, *Coord. Chem. Rev.*, 2016, **306**, 636–651. (e) F. Dumur, *Org. Electron.*, Recent advances in organic light-emitting devices comprising copper complexes: A realistic approach for low-cost and highly emissive devices?, 2015, **21**, 27–39. (f) S. Singha, D. Kim, H. Seo, S. W. Cho and K. H. Ahn, Fluorescence sensing systems for gold and silver species, *Chem. Soc. Rev.*, 2015, **44**, 4367–4399. (g) V. W.-W. Yam, V. K.-M. Au and S. Y.-L. Leung, Light-Emitting Self-Assembled Materials Based on d8 and d10 Transition Metal Complexes, *Chem. Rev.*, 2015, **115**, 7589-7728.

2 (a) R. Hamze, J. L. Peltier, D. Sylvinson, M. Jung, J. Cardenas, R. Haiges, M. Soleilhavoup, R. Jazzar, P. I. Djurovich, G. Bertrand and M. E. Thompson, Eliminating nonradiative decay in Cu(I) emitters: >99% quantum efficiency and microsecond lifetime, *Science*, 2019, **363**, 601. (b) Z. Wang, J. Zhu, Z. Liu, P. Wu, H. Wang, Z. Zhang and B. Wei, Thermally activated delayed fluorescence of co-deposited copper(i) complexes: cost-effective emitters for highly efficient organic light-emitting diodes, *J. Mater. Chem. C*, 2017, **5**, 6982-6988. (c) M. El Sayed Moussa, S. Evariste, H. L. Wong, L. Le Bras, C. Roiland, L. Le Polles, B. Le Guennic, K. Costuas, V. W. W. Yam and C. Lescop, A solid state highly emissive Cu(i) metallacycle: promotion of cuprophilic interactions at the excited states, *Chem. Commun.*, 2016, **52**, 11370-11373. (d) S. Pal, B. Sen, S. Lohar, M. Mukherjee, S. Banerjee and P. Chattopadhyay, Effect of metal oxidation state on FRET: a Cu(i) silent but selectively Cu(ii) responsive fluorescent reporter and its bioimaging applications, *Dalton Trans.*, 2015, **44**, 1761-1768. (e) X.-L. Xin, M. Chen, Y.-b. Ai, F.-l. Yang, X.-L. Li and F. Li, Aggregation-Induced Emissive Copper(I) Complexes for Living Cell Imaging, *Inorg. Chem.*, 2014, **53**, 2922-2931.

3 (a) F. Lin, W. Liu, H. Wang and J. Li, Strongly emissive white-light-emitting silver iodide based inorganic–organic hybrid structures with comparable quantum efficiency to commercial phosphors, *Chem. Commun.*, 2020, **56**, 1481-1484. (b) M. Z. Shafikov, R. Czerwieniec and H. Yersin, Ag(i) complex design affording intense phosphorescence with a landmark lifetime of over 100 milliseconds, *Dalton Trans.*, 2019, **48**, 2802-2806. (c) A. S. Romanov, S. T. E. Jones, L. Yang, P. J. Conaghan, D. Di, M. Linnolahti, D. Credgington and M. Bochmann, Mononuclear Silver Complexes for Efficient Solution and Vacuum-Processed OLEDs, *Adv. Opt. Mater.*, 2018, **6**, 1801347. (d) M. Z. Shafikov, A. F. Suleymanova, R. Czerwieniec and H. Yersin, Design Strategy for Ag(I)-Based Thermally Activated Delayed Fluorescence Reaching an Efficiency Breakthrough, *Chem. Mater.*, 2017, **29**, 1708-1715. (e) J. Chen, T. Teng, L. Kang, X.-L. Chen, X.-Y. Wu, R. Yu and C.-Z. Lu, Highly Efficient Thermally Activated Delayed Fluorescence in Dinuclear Ag(I) Complexes with a Bis-Bidentate Tetraphosphane Bridging Ligand, *Inorg. Chem.*, 2016, **55**, 9528-9536. (f) D. Kakizoe, M. Nishikawa, T. Degawa and T. Tsubomura, Intense blue emission and a reversible hypsochromic shift of luminescence caused by grinding based

on silver(i) complexes, *Inorg. Chem. Front.*, 2016, **3**, 1381-1387.
4 (a) R. Visbal, I. Ospino, J. M. López-de-Luzuriaga, A. Laguna and M. C. Gimeno, N-Heterocyclic Carbene Ligands as Modulators of Luminescence in Three-Coordinate Gold(I) Complexes with Spectacular Quantum Yields, *J. Am. Chem. Soc.*, 2013, **135**, 4712-4715. (b) R. Czerwieniec, T. Hofbeck, O. Crespo, A. Laguna, M. Concepción Gimeno and H. Yersin, The Lowest Excited State of Brightly Emitting Gold(I) Triphosphine Complexes, *Inorg. Chem.*, 2010, **49**, 3764-3767.
5 S. G. Patra, S. De, D. A. Tocher and D. Datta, Photophysics of a mono-nuclear tetrahedral silver(I)N4 core and its copper(I) analog, *Inorg. Chim. Acta*, 2018, **471**, 649-657.
6 (a) R. Hamze, S. Shi, S. C. Kapper, D. S. Muthiah Ravinson, L. Estergreen, M.-C. Jung, A. C. Tadle, R. Haiges, P. I. Djurovich, J. L. Peltier, R. Jazzar, G. Bertrand, S. E. Bradforth and M. E. Thompson, "Quick-Silver" from a Systematic Study of Highly Luminescent, Two-Coordinate, d10 Coinage Metal Complexes, *J. Am. Chem. Soc.*, 2019, **141**, 8616-8626; (b) L.-R. Xing, Z. Lu, M. Li, J. Zheng and D. Li, Revealing High-Lying Intersystem Crossing in Brightly Luminescent Cyclic Trinuclear CuI/AgI Complexes, *J. Phys. Chem. Lett.*, 2020, **11**, 2067-2073. (c) A. A. Titov, O. A. Filippov, A. F. Smol'yakov, I. A. Godovikov, J. R. Shakirova, S. P. Tunik, I. S. Podkorytov and E. S. Shubina, Luminescent Complexes of the Trinuclear Silver(I) and Copper(I) Pyrazolates Supported with Bis(diphenylphosphino)methane, *Inorg. Chem.*, 2019, **58**, 8645-8656. (d) M. Osawa, M. Hashimoto, I. Kawata and M. Hoshino, Photoluminescence properties of TADF-emitting three-coordinate silver(i) halide complexes with diphosphine ligands: a comparison study with copper(i) complexes, *Dalton Trans.*, 2017, **46**, 12446-12455. (e) M. Osawa, I. Kawata, R. Ishii, S. Igawa, M. Hashimoto and M. Hoshino, Application of neutral d10 coinage metal complexes with an anionic bidentate ligand in delayed fluorescence-type organic light-emitting diodes, *J. Mater. Chem. C*, 2013, **1**, 4375-4383. (f) T. S. Teets, D. V. Partyka, A. J. Esswein, J. B. Updegraff, M. Zeller, A. D. Hunter and T. G. Gray, Luminescent, Three-Coordinate Azadipyrromethene Complexes of d10 Copper, Silver, and Gold, *Inorg. Chem.*, 2007, **46**, 6218-6220.
7 C.-W. Hsu, C.-C. Lin, M.-W. Chung, Y. Chi, G.-H. Lee, P.-T. Chou, C.-H. Chang and P.-Y. Chen, Systematic Investigation of the Metal-Structure–Photophysics Relationship of Emissive d10-Complexes of Group 11 Elements: The Prospect of Application in Organic Light Emitting Devices, *J. Am. Chem. Soc.*, 2011, **133**, 12085-12099.
8 E. Yu-Tzu Li, T.-Y. Jiang, Y. Chi and P.-T. Chou, Semi-quantitative assessment of the intersystem crossing rate: an extension of the El-Sayed rule to the emissive transition metal complexes, *PCCP*, 2014, **16**, 26184-26192.
9 F. Li, R.-B. Lin, Y.-S. Wei, P.-Q. Liao, J. Bai, W. Xue, W.-X. Zhang, J.-P. Zhang and X.-M. Chen, Metal-ion controlled solid-state reactivity and photoluminescence in two isomorphous coordination polymers, *Inorg. Chem. Front.*, 2014, **1**, 172-177.
10 J. Pospisil, I. Jess, C. Näther, M. Necas and P. Taborsky, Luminescence properties of "double-stranded staircase" copper(i) halide coordination polymers with N-containing ligands, *New J. Chem.*, 2011, **35**, 861-864.
11 P. C. Ford, E. Cariati and J. Bourassa, Photoluminescence Properties of Multinuclear Copper(I) Compounds, *Chem. Rev.*, 1999, **99**, 3625-3648.
12 C. Wölper, M. D. P. Bastardes, I. Dix, D. Kratzert and P. G. Jones, A simple system with many structural variants: a reexamination of (amine)halogenidosilver(I) complexes, *Z. Naturforsch., B: J. Chem. Sci.*, 2010, **65**, 647-673.
13 D. Yang, W. Xu, X. Cao, S. Zheng, J. He, Q. Ju, Z. Fang and W. Huang, Two Silver Coordination Network Compounds with Colorful Photoluminescence, *Inorg. Chem.*, 2016, **55**, 7954-7961.
14 J. Zhang, Y. Wang, W. Chen, L. Long and C. Zhang, Three Distinct Silver(I) Coordination Polymers: Bridging-Ligand Directed Syntheses, Crystal Structures, Luminescence, and Nitrobenzene Sensing Properties, *Z. Anorg. Allg. Chem.*, 2015, **641**, 1366-1373.
15 Q.-X. Liu, F.-B. Xu, Q.-S. Li, X.-S. Zeng, X.-B. Leng, Y. L. Chou and Z.-Z. Zhang, A Luminescent Silver(I) Carbene Stair Polymer, *Organometallics*, 2003, **22**, 309-314.
16 K. Kumar Bisht, A. Cherian Kathalikkattil and E. Suresh, Structure modulation, argentophilic interactions and photoluminescence properties of silver(i) coordination polymers with isomeric N-donor ligands, *RSC Adv.*, 2012, **2**, 8421-8428.
17 E. Lucenti, E. Cariati, A. Previtali, D. Marinotto, A. Forni, V. Bold, V. C. Kravtsov, M. S. Fonari, S. Galli and L. Carlucci, Versatility of Cyclic Triimidazole to Assemble 1D, 2D, and 3D Cu(I) Halide Coordination Networks, *Cryst. Growth Des.*, 2019, **19**, 1567-1575.
18 E. Lucenti, A. Forni, C. Botta, L. Carlucci, C. Giannini, D. Marinotto, A. Previtali, S. Righetto and E. Cariati, H-Aggregates Granting Crystallization-Induced Emissive Behavior and Ultralong Phosphorescence from a Pure Organic Molecule, *J. Phys. Chem. Lett.*, 2017, **8**, 1894-1898.
19 Z. An, C. Zheng, Y. Tao, R. Chen, H. Shi, T. Chen, Z. Wang, H. Li, R. Deng, X. Liu and W. Huang, Stabilizing triplet excited states for ultralong organic phosphorescence, *Nat. Mater.*, 2015, **14**, 685-690.
20 A. Forni, E. Lucenti, C. Botta and E. Cariati, Metal free room temperature phosphorescence from molecular self-interactions in the solid state, *J. Mater. Chem. C*, 2018, **6**, 4603-4626.
21 L. M. Engelhardt, S. Gotsis, P. C. Healy, J. D. Kildea, B. W. Skelton and A. H. White, Lewis-Base Adducts of Group 11 Metal(I) Compounds. XLV. Conformational Systematics of $[(N\text{-base})_1(AgX)_1]_n$ Complexes. *Aust. J. Chem.*, 1989, **42**, 149–176.
22 (a) E. Lucenti, A. Forni, C. Botta, L. Carlucci, C. Giannini, D. Marinotto, A. Pavanello, A. Previtali, S. Righetto and E. Cariati, Cyclic Triimidazole Derivatives: Intriguing Examples of Multiple Emissions and Ultralong Phosphorescence at Room Temperature, *Angew. Chem. Int. Ed.*, 2017, **56**, 16302-16307. (b) E. Lucenti, A. Forni, C. Botta, L. Carlucci, A. Colombo, C. Giannini, D. Marinotto, A. Previtali, S. Righetto and E. Cariati, The Effect of Bromo Substituents on the Multifaceted Emissive and Crystal-Packing Features of Cyclic Triimidazole Derivatives, *ChemPhotoChem*, 2018, **2**, 801-805. (c) E. Lucenti, A. Forni, C. Botta, C. Giannini, D. Malpicci, D. Marinotto, A. Previtali, S. Righetto and E. Cariati, Intrinsic and Extrinsic Heavy-Atom Effects on the Multifaceted Emissive Behavior of Cyclic Triimidazole, *Chem. Eur. J.*, 2019, **25**, 2452-2456. (d) A. Previtali, E. Lucenti, A. Forni, L. Mauri, C. Botta, C. Giannini, D. Malpicci, D. Marinotto, S. Righetto and E. Cariati, Solid State Room Temperature Dual Phosphorescence from 3-(2-Fluoropyridin-4-yl)triimidazo[1,2-a:1',2'-c:1",2"-e][1,3,5]triazine, *Molecules*, 2019, **24**, 2552. (e) E. Lucenti, A. Forni, A. Previtali, D. Marinotto, D. Malpicci, S. Righetto, C. Giannini, T. Virgili, P. Kabacinski, L. Ganzer, U. Giovanella, C. Botta and E. Cariati, Unravelling the intricate photophysical behavior of 3-(pyridin-2-yl)triimidazotriazine AIE and RTP polymorphs, *Chem. Sci.*, 2020, **11**, 7599-7608.
23 (a) A. Forni, S. Pieraccini, S. Rendine and M. Sironi, Halogen bonds with benzene: An assessment of DFT functionals, *J. Comput. Chem.*, 2014, **35**, 386-394. (b) A. Forni, S. Pieraccini, S. Rendine, F. Gabas and M. Sironi, Halogen-bonding interactions with π systems: CCSD(T), MP2, and DFT calculations, *ChemPhysChem*, 2012, **13**, 4224-4234. (c) A. Forni, S. Pieraccini, D. Franchini and M. Sironi, Assessment of

View Article Online
DOI: 10.1039/D0QI01377C

View Article Online
DOI: 10.1039/D0QI01377C

DFT Functionals for QTAIM Topological Analysis of Halogen Bonds with Benzene, *J. Phys. Chem A*, 2016, **120**, 9071-9080.

24 M. Majoube, M. Henry, L. Chinsky and P. Y. Turpin, Preresonance Raman spectra for imidazole and imidazolium ion: interpretation of the intensity enhancement from a precise assignment of normal modes, *Chem. Phys.*, 1993, **169**, 231-241.

25 E. Cariati, A. Forni, E. Lucenti, D. Marinotto, A. Previtali, S. Righetto, C. Botta, V. Bold, V. Kravtsov and M. S. Fonari, Extrinsic Heavy Metal Atom Effect on the Solid-State Room Temperature Phosphorescence of Cyclic Triimidazole, *Chem. Asian J.*, 2019, **14**, 853-858.

26 R. F. W. Bader, Atoms in Molecules: a Quantum Theory. In *International Series of Monographs on Chemistry 22*; Oxford University Press: Oxford, 1990.

27 A. Serpe, F. Artizzu, L. Marchiò, M. L. Mercuri, L. Pilia and P. Deplano, Argentophilic Interactions in Mono-, Di-, and Polymeric Ag(I) Complexes with N,N'-Dimethyl-piperazine-2,3-dithione and Iodide, *Cryst. Growth Des.*, 2011, **11**, 1278-1286.

28 (a) H. Schmidbaur and A. Schier, Argentophilic Interactions, *Angew. Chem. Int. Ed.*, 2015, **54**, 746-784. (b) L. Ray, M. M. Shaikh and P. Ghosh, Shorter Argentophilic Interaction than Aurophilic Interaction in a Pair of Dimeric $\{(NHC)MCl\}_2$ (M = Ag, Au) Complexes Supported over a N/O-Functionalized N-Heterocyclic Carbene (NHC) Ligand, *Inorg. Chem.*, 2008, **47**, 230-240.

29 (a) M. O'Keeffe, M. A. Peskov, S. J. Ramsden and O. M. Yaghi, The Reticular Chemistry Structure Resource (RCSR) Database of, and Symbols for, Crystal Nets, *Acc. Chem. Res.*, 2008, **41**, 1782-1789. (b) C. Bonneau, M. O'Keeffe, D. M. Proserpio, V. A. Blatov, S. R. Batten, S. A. Bourne, M. S. Lah, J.-G. Eon, S. T. Hyde, S. B. Wiggin and L. Öhrström, Deconstruction of Crystalline Networks into Underlying Nets: Relevance for Terminology Guidelines and Crystallographic Databases. *Cryst. Growth Des.*, 2018, **18**, 3411-3418.